On How Copper Mordenite Properties Govern the Framework Stability and Activity in the Methane-to-Methanol Conversion

On how Copper Mordenite Properties govern the Framework Stability and Activity in the Methane-to-Methanol Conversion

Michael Dyballa,[a,b,‡,*] Dimitrios K. Pappas,[a] Karoline Kvande,[a] Elisa Borfecchia,[c,d,†] Bjørnar Arstad,[b] Pablo Beato,[c,*] Unni Olsbye,[a] and Stian Svelle[a,*]

[a]*Center for Materials Science and Nanotechnology (SMN), Department of Chemistry, University of Oslo, 1033 Blindern, 0315 Oslo (Norway)*
[b]*SINTEF Industry, Forskningsveien 1, 0373 Oslo (Norway)*
[c]*Haldor Topsøe A/S, Nymøllevej 55, 2800 Kgs. Lyngby (Denmark)*
[d]*Department of Chemistry and INSTM Reference Center, University of Turin, via P. Giuria 7, 10125 Turin (Italy)*

Present Addresses:
‡ *Institute of Chemical Technology, University of Stuttgart, Pfaffenwaldring 55, 70569 Stuttgart (Germany)*
† *Center for Materials Science and Nanotechnology (SMN), Department of Chemistry, University of Oslo, 1033 Blindern, 0315 Oslo (Norway)*

* *Corresponding authors:*

Michael Dyballa; E-mail: michael.dyballa@itc.uni-stuttgart.de

Pablo Beato; E-mail: pabb@topsoe.com

Stian Svelle; E-mail: stian.svelle@smn.uio.no

Abstract

Herein we investigate the activity of copper mordenites in the methane-to-methanol conversion and the material de- and realumination. From four parent materials, a library of copper mordenites was synthesized by liquid and solid state ion exchange techniques. Two key properties govern the activity of these materials in the methane conversion: the parent counter ion and the copper ion exchange procedure. H-form parents result in more active materials. The optimum stoichiometry between silicon, aluminum and copper leads to a methanol productivity of up to 169 µmol/g. This equals to a stoichiometry of up to 0.47 methanol molecules formed per copper atom. The methanol productivity is constant over up to three cycles. The stability of the mordenite framework was monitored by SEM, EDX, ^{27}Al and ^{29}Si MAS NMR spectroscopy. No detectable copper nanoparticles formed. However, a dealumination of the mordenite framework and the formation of extra-framework aluminum (EFAl) species in quantities of up to 12 % were observed on H-form copper mordenites. The dealumination is weak or completely inhibited if counter ions like Na^+ or Cu^{2+} are present. These ions stabilize the framework aluminum during the reaction steps and upon heat treatments. Notably, the most active materials have significant EFAl contents present.

Keywords

Cu-MOR, Methane activation, MAS NMR, De-/Realumination, Methanol

1. Introduction

Groothaert et al.[1] proposed a three step process utilizing Cu-ZSM-5 and Cu-MOR zeolites for the direct conversion of methane to methanol. A typical process cycle starts with the zeolite activation in O_2 at 773 K followed by the loading with methane at 473 K. The C-H bond cleavage results in a methoxy group, that is, subsequently hydrolyzed at 473 K and extracted in the form of the oxygenate e.g. methanol. The nuclearity of the active copper species in MOR zeolite depends on multiple factors. In particular dicopper[2-6] and tricopper[7] species balanced in between framework aluminum sites have been found in Mordenite. Even higher copper site nuclearities have been suggested.[8] DFT calculations revealed that mainly the aluminum content and the localization of acid sites in the framework impact on the stability and the formation of a specific copper motif. Through an extensive study of different topologies, Park et al.[9] found that many zeolites with an 8-membered ring motif are able to convert methane into methanol using various copper-oxo sites. Especially MOR and MAZ based zeolites exhibited high productivities due to 8-membered rings with 2 Al atoms (2Al 8-MR) in the framework structures. On the other hand it was reported that 2Al 6-MR motifs inhibit the redox activity of copper in frameworks with CHA[10-11] and SZR[12] topology. Recently, *operando* X-Ray Absorption Spectroscopy (XAS) revealed strong similarities in the average structural and electronic properties of copper sites in copper exchanged CHA and MOR materials monitored during the stepwise methane conversion.[13]

It is of particular interest how to tune zeolite properties for a maximum methanol production. The mordenite topology consists of straight 12-MR membered ring channels with diameter 7.0 x 6.5 Å and perpendicular 8-MR side pockets with diameter 5.7 x 2.6 Å. Grundner et al.[7] identified a 2Al containing motif in this 8-MR side pocket as the copper bearing site. This site lead to a methanol productivity of up to 160 µmol/g (about 0.31-0.33 mol_{CH3OH}/mol_{Cu}) and is the highest reported so far for Cu,H-MOR zeolites with n_{Si}/n_{Al} ratio 7.2.[7] The authors combined IR and X-Ray spectroscopy with DFT calculations to support the formation of a single trinuclear copper-oxo site of type $[Cu_3(\mu\text{-}O)_3]^{2+}$. Special emphasis was given to the fact that the liquid ion exchange (LIE) with copper was conducted below pH 6 to avoid copper precipitation and to enhance the amount of single charged $[Cu^{II}(H_2O)_5OH]^+$ complexes. The single positive charge prevents the copper from bridging two acid sites and yields mainly Cu-OH groups after activation. In another article, these authors compared several counter ions and concluded that materials derived from H-MOR parent zeolites showed superior methanol productivity over up to 8 cycles.[14]

Le et al.[15] compared LIE and solid state ion exchanged (SSIE) mordenites in the methane oxidation reaction. For the SSIE, $Cu^{I}Cl$ and $Cu^{II}(acac)_2$ were used. All solid-state ion exchanged materials exhibited a higher methanol productivity than the corresponding LIE of Na^+ and NH_4^+ mordenite materials. The highest activity of 60 µmol/g_{Cu} (equal 0.22 mol_{CH3OH}/mol_{Cu}) was observed for a Cu,H-

MOR zeolite with 1 wt% copper. In higher exchange degrees, the activity dropped below 0.1 mol_{CH3OH}/mol_{Cu} and the zeolites turned grey. This color change is indicative of copper nanoparticle formation. The better performance of SSIE over LIE was explained by the size of the $[Cu^{II}(H_2O)_6]^{2+}$ complex, being too big to enter the small 8-MR side pockets of the mordenite. SSIE with $Cu^{II}(acac)_2$ outperformed the exchange with $Cu^{I}Cl$ as a result of an incomplete or inhomogeneous exchange leading to the formation of bulk CuO using the latter copper salt for the exchange. This was verified by Bozbag et al.[16] who investigated the SSIE of H-MOR with $Cu^{I}Cl$ without prior calcination. This led to a subsequent increase in methanol output over multiple reaction cycles and a maximum methanol productivity of 23 $\mu mol_{CH3OH}/g_{Cu}$. The micropore volume decreased significantly upon the SSIE. By applying transmission electron microscopy (TEM) it was verified that nanoparticles had formed. The formed nanoparticles have been proposed by Tomkins et al. [17] to participate in the methane conversion at high pressure, whereas the ambient pressure reaction requires active sites with low nuclearity (Cu dimers or small clusters).

The stepwise methane-to-methanol conversion is governed by stoichiometry, meaning that the n_{Si}/n_{Al} and n_{Cu}/n_{Al} ratios as well as the nuclearity of the active species define the total yield. The framework stability was scarcely investigated until now despite the fact that stoichiometric considerations depend heavily in the amount of framework aluminum. In Zeolites, tetrahedral coordinated aluminum generates ion-exchangeable acid sites.[18] Dealumination, i.e. release of tetrahedrally coordinated framework aluminum and formation of octahedrally coordinated extra framework aluminum (EFAl) in the zeolite pores is accompanied by the loss of an equal quantity of bridging Si(OH)Al-groups.[19] This changes significantly the stoichiometry between copper and 2Al sites and thus influences the formation of the number of active sites. A dealumination of Cu-MOR was proven indirectly by FT-IR (hinting to an EFAl content of >6%) but to our knowledge no in depth investigation on individual samples was conducted.[14] In another work on carbonylation of methanol Al-OH groups attributed to EFAl species were found using FT-IR on Cu-MOR [20] Narsimhan et al.[21] investigated LIE prepared Cu-MOR zeolites in the methane activation and subsequent carbonylation to acetic acid and assumed that no EFAl was present in the Cu-MOR framework. Techniques of choice to investigate the dealumination of zeolites are ^{27}Al and ^{29}Si MAS NMR spectroscopy, as demonstrated already in the early 80s.[22-25] Reviews on this topic have been published as well by Engelhardt[26] and Fyfe et al.[27]

In Cu loaded zeolites, care must be taken due to Cu ions that are/might be paramagnetic due to unpaired electrons. Paramagnetic centers will influence nearby atoms in various ways depending on the nature of their coordination. The paramagnetic ion itself is not observable by NMR but may lead to peak position shifts, line broadening and enhanced relaxation rates depending on the strength of

interactions. A critical factor is whether the paramagnetic ion is in a bonding network with nearby atoms. In such cases there is a strong influence as exemplified by NMR of metals where the free electrons in the conducting band results in a shift of many hundred ppm of the peaks (Knight shift). This is due to a small but significant electron density at the NMR nuclei from the delocalized conducting electrons. Similarly, in otherwise diamagnetic compounds, overlap of electron density through s-like orbitals from the paramagnetic center onto the NMR active nuclei will also lead to peak position shifts. These types of shifts are described by the Fermi contact interaction. If the paramagnetic ion is not (covalently) bonded to nearby atoms the influence is less strong, especially if the distance is some Angstroms. In such cases only a reduced T1 relaxation time constant would be measured. However, by strong enough interactions a heavy line broadening with a spinning sideband manifold would be present due to electron-nuclei dipole-dipole interactions. If the interactions described above are strong enough the NMR signal will eventually vanish. Li et al.[28] recently demonstrated the increasing influence of paramagnetic Eu^{2+} doped into a series of SrH_2 ($Sr_{1-x}Eu_xH_2$). From ^1H MAS NMR they showed that the influence of paramagnetic Eu^{2+} ion on nearby atoms lead to a sphere with strongly perturbed atoms, characterized by a "wipe out radius" of 1.7 nm.[28] Despite possible complications MAS NMR investigations is often successfully conducted on materials with paramagnetic centers as summarized in an excellent review written by Grey and Dupré.[29] In fact, the interactions that might complicate the NMR spectra also lead to more parameters to work with when characterizing the materials as presence or absence of peak shape distortions are keys to understand the systems. In the case of our Cu loaded zeolites most framework atoms are not bonded directly to the Cu and hence only modest influence (lower T1 values) is expected.

A few studies have touched upon the paramagnetic influence of Cu on the Al and Si atoms. A broadening of the EFAl peak of octahedral coordinated aluminum at 0 ppm in the ^{27}Al MAS NMR spectra of Cu-SSZ-13 (8-membered ring (MR) pores, *chab* cages) was shown by Beale et al.[30] A combination of ^{27}Al and ^{29}Si MAS NMR spectroscopy was successfully applied to investigate the framework of zeolite Cu-Y (12-MR pores) without observing a significant line broadening of the respective ^{27}Al and ^{29}Si peaks.[31] A significantly lowered T1 spin-lattice relaxation time constant for the return of equilibrium magnetization of ^{13}C and ^{29}Si nuclei in these samples, due to a paramagnetic relaxation enhancement, was used to drastically increase the sensitivity of the MAS NMR measurements. Inagaki et al.[32] explained the absence of line broadening of ^{29}Si nuclei upon Cu^{2+} doping with a maintained T2 relaxation time since the electronic relaxation time of Cu^{2+} is in the order of the Zeeman interaction (10^{-8} s^{-1}). The range of the effect was determined to be in the order of more than 1 nm.[32] Palamara et al.[33] used the paramagnetic sensitivity enhancement to

determine the distribution of copper in H- and Na-form zeolites SSZ-13 and Y. Song et al.[34] recently used a combination of ^{27}Al and ^{29}Si MAS NMR spectroscopy to investigate the dealumination of Cu-SSZ-13 catalysts used for De-NO_x applications.

In the present study, we address the methanol productivity of a vast library of Cu-MOR materials. We vary material properties like counter ion, ion exchange procedure, n_{Cu}/n_{Al} ratio, and framework n_{Si}/n_{Al} ratio. The methanol production and the framework stability are additionally monitored over multiple reaction cycles. We summarize claims from literature regarding important synthesis parameters and identify the preferred synthesis route. For the first time we quantitatively monitor the dealumination of the zeolite framework using ^{27}Al and ^{29}Si MAS NMR spectroscopy over up to three reaction cycles and evaluate the impact of n_{Si}/n_{Al} ratio, n_{Cu}/n_{Al} ratio, and synthesis route. This approach leads to highly active materials and a better understanding of the stoichiometry in the methane-to-methanol conversion.

2. Experimental Section

2.1. Material synthesis

Zeolite materials CBV21A (NH_4-MOR/11) and CBV10ADS (Na-MOR/7) were purchased from Zeolyst. The starting materials were exchanged into their proton or sodium form. The materials were prior to any use exchanged at 333 K with solutions of 10 wt% NH_4NO_3 or $NaNO_3$ (both Sigma-Aldrich), respectively, and washed with demineralized water until nitrate-free. To get the H-forms of the materials, the ammonia was burned off by calcining the materials at 773 K for 8 h, applying a ramp rate less than 1 K/min. A pH treatment of parent H-form zeolites was conducted by stirring them for 16 h in 60 ml/g water solution with thepH adjusted to 5.2 – 5.7 using NH_4OH-solution (28 wt%, Sigma–Aldrich). The NH_4-form of Na-MOR/7 was a result of three consecutive liquid ion exchange (LIE) steps with 10 wt% NH_4NO_3 in distilled water followed by four washing steps. To synthesize Na-MOR/11, the precursor H-MOR/11 was three times exchanged by LIE at 333 K with 10 wt% $NaNO_3$ in distilled water. LIE with copper was performed as follows: copper(II)acetate ($CuAc_2$, Sigma-Aldrich) was diluted in distilled water (concentration between 0.002 and 0.02 M, see Table 1). The parent material was added to the solution (at ratio 60 ml/g) and the pH adjusted to 5.2 – 5.7 using NH_4OH-solution (28 wt%, Sigma–Aldrich). The materials were then stirred at RT for 16 h, the solution removed by centrifugation and the material washed at least three times to remove surplus Cu(II) ions. Solid state ion exchange (SSIE) of H-MOR materials was performed by pore-impregnating the dried material with a water-solution containing the desired copper salt concentration. Afterwards, for $CuCl_2 \cdot 2H_2O$ (Sigma-Aldrich), the materials were calcined at 773 K for 16.5 h in N_2 (120 ml/min). For $CuAc_2$, the materials were calcined at 773 K for 16.5 h in synthetic

air (120 ml/min) followed by 8.5 h in N_2 (120 ml/min). For some catalysts, a severe heat treatment was conducted by calcining them for 30 h at 823 K in air.

2.2. Characterization

X-ray diffraction (XRD) patterns were measured on a Bruker D8 Discovery diffractometer using Cu-Kα radiation (λ = 1.5418 Å). The patterns were collected in a 2Θ range from 2 to 70° in Bragg-Brentano geometry. N_2-Physisorption was conducted using a BELsorp mini instrument at 77 K. Prior to the measurements, the materials were activated in vacuum for 1 h at 353 K and 2 h at 573 K. The specific surface areas were calculated using the Brunauer-Emmett-Teller approximation (BET) in a p/p_0= range up to 0.1. Scanning electron microscopy (SEM) and high angle backscattering electron (BSE) images were taken on a Hitachi SU8230 instrument. The elemental composition, n_{Si}/n_{Al} ratio and n_{Cu}/n_{Al} ratio, were determined by energy-disperse X-ray spectroscopy (EDX) at 20 kV accelerating voltage on 200x200 µm areas of pelletized material. Quantification was performed using the Bruker Quantax system consisting of a X-flash 6|10 detector and Esprit software. The water content of the materials was determined using a Stanton Redcroft TGA instrument by heating the materials at 1 K/min to 573 K in dry synthetic air and maintaining that temperature for 1.5 h.

^{27}Al and ^{29}Si MAS NMR spectra were collected using a Bruker Avance III spectrometer operating at a magnetic field of 11.74 T at SINTEF, Oslo (NO). For the ^{27}Al spectra we used a 3.2 mm triple resonance MAS probe at a MAS rate of 20 KHz and for the ^{29}Si spectra we used a 4 mm double resonance probe at a MAS rate of 10 KHz. The applied ^{27}Al and ^{29}Si resonance frequencies at this field was 130.3 MHz and 99.4 MHz, respectively. Some spectra reported in the Supporting Information (SI) were collected using different setups, further details are reported in figure captions when necessary. All NMR experiments were of the single-pulse type, i.e. a recovery time followed by a pulse and acquisition of the electric signal (free induction decay, FID). A total of 10000 FIDs were accumulated and averaged for the Al spectra using a recovery time of 0.5 s and a pulse length of 0.44 µs. At our RF-field of 94.4 kHZ, this corresponds to a π/12 pulse in a 1M $Al(NO_3)_3$ water solution. With such parameters we can expect fair ratios between the peak areas of tetrahedral and octahedral coordinated Al if rather similar peak shapes are observed, i.e. low quadrupolar coupling strengths. For each Si spectra a total of 1800 FIDs were accumulated using 90 ° pulses (each of 7 µs length at a RF-field of 35.7 kHz) and a recovery time of 30 s. Before Fourier transform of the averaged FIDs zero filling and apodization were applied to improve line shape definitions and signal to noise. The apodization were done by multiplying the FIDs with a decaying exponential window

function with a processing line broadening (LB) factor of 20 Hz. All NMR spectra were then adjusted by proper signal phasing and baseline corrections.

Temperature-programmed decomposition of *n*-propylamine was measured on ca. 25 mg of zeolite in sieve fraction 250 to 425 μm.[35] The material was placed in a glass reactor (ID = 11 mm) forming a solid bed. The material was activated in oxygen at 823 K for 30 min and subsequently cooled down to 423 K. A stream of N_2 was saturated with *n*-propylamine using a bubble saturator was passed through the reactor for 20 min. The material was flushed for 1 h with N_2 to desorb surplus *n*-propylamine. The temperature was then increased at 20 K/min up to 823 K. Upon thermal decomposition at acid sites propene (and ammonia) formed and was quantified using an online Pfeiffer Omnistar quadrupole mass spectrometer.

2.3. Catalytic testing

The materials were tested in the conversion of methane to methanol in a quartz fixed bed reactor (i.d. = 6 mm) as described before.[11] Briefly, 100 mg of material, corrected for the water content, with uniform particle size in the range of 250 to 425 μm were used for each experiment. The stepwise conversion consists of the following steps: 1) activation in oxygen; 2) reaction with methane; 3) extraction of methanol with water. First, the material was dried in helium flow (15 ml/min) at 423 K; then an O_2 flow (15 ml/min) was introduced and the temperature was increased with 5 K/min to 773 K, and kept for 480 min. After activation, the temperature was decreased to 473 K with a rate of 5 K/min in O_2. The material was purged with helium for 60 min, and then CH_4 was introduced at a flow of 15 ml/min for 360 minutes at 473 K. The material was again purged with helium. Finally a H_2O-saturated flow (318 K, p_{H2O} = 9.1 kPa) of neon/helium (15 ml/min) was introduced in the reactor at 473 K. The effluent was analysed by coupled gas chromatography/mass spectroscopy using a Hewlett Packard 6890/5972 GC-MS system.

3. Results and Discussion

3.1. Properties of parent H-MOR and Na-MOR zeolites

All our copper materials were synthesized from the parent mordenite zeolites H-MOR/11, Na-MOR/11, H-MOR/7 and Na-MOR/7 (see Table 1). The two H-MOR zeolites show a larger BET surface area compared to the Na-MOR zeolites. All parent zeolites were investigated by XRD (see Figure S1 in the supporting information, SI). The powder patterns reveal pure MOR frameworks without competing phases or significant amorphicity. Investigation by SEM (see Figure S2 in the SI) revealed partially aggregated zeolite crystals in the dimension 50 - 300 nm. Because of the small

crystal size, the chemical composition could be determined by EDX spectroscopy resulting in identical n_{Si}/n_{Al} ratios in both H- and Na-form. The Brønsted acid site density (ASD) of the parent MOR zeolites was investigated using thermal decomposition of *n*-propylamine to be as follows: H-MOR/11 (1.1 mmol/g), Na-MOR/11 (0.1 mmol/g), H-MOR/7 (2.0 mmol/g) and Na-MOR/7 (0.1 mmol/g). Compared to the expected values at n_{Si}/n_{Al} ratios 11 (1.4 mmol/g) and 7 (2.1 mmol/g), most acidic Si(OH)Al-groups in the parent H-MOR are accessible by n-propyleamine.

Table 1: Summary of synthesis and characterization data of herein discussed MOR zeolites. The exchange method and, if applicable, molarity of the exchange solution is indicated under "exchange".

material	exchange conditions	n_{Si}/n_{Al} ratio[1]	n_{Cu}/n_{Al} ratio[1]	Cu [wt%]	BET [m^2/g]	V_{tot} [ml/g][2]
H-MOR/11	-	11	-	-	530	0.29
0.13Cu,H-MOR/11	LIE, 0.0025	11	0.13	1.16	470	0.30
0.19Cu,H-MOR/11	LIE, 0.005	11	0.19	1.67	450	0.29
0.28Cu,H-MOR/11	LIE, 0.01	11	0.28	2.47	470	0.31
0.36Cu,H-MOR/11	LIE, 0.02	11	0.36	3.18	460	0.30
0.09Cu,H-MOR/11/Cl	SSIE	11	0.09	0.81	530	0.33
0.35Cu,H-MOR/11/Cl	SSIE	11	0.35	3.08	530	0.33
0.09Cu,H-MOR/11/Ac	SSIE	11	0.09	0.83	500	0.34
0.35Cu,H-MOR/11/Ac	SSIE	11	0.35	3.07	500	0.30
Na-MOR/11	-	11	-	-	500	0.30
0.18Cu,Na-MOR/11	LIE, 0.0025	11	0.18	1.58	500	0.31
0.24Cu,Na-MOR/11	LIE, 0.005	11	0.24	2.06	500	0.31
0.32Cu,Na-MOR/11	LIE, 0.01	11	0.32	2.83	500	0.31
H-MOR/7	-	7	-	-	520	0.26
0.06Cu,H-MOR/7	LIE, 0.002	7	0.06	0.97	490	0.27
0.14Cu,H-MOR/7	LIE, 0.005	7	0.14	1.78	450	0.27
0.18Cu,H-MOR/7	LIE, 0.01	7	0.18	2.33	440	0.25
0.24Cu,H-MOR/7	LIE, 0.02	7	0.24	3.20	440	0.25
Na-MOR/7	-	7	-	-	480	0.24
0.13Cu,Na-MOR/7	LIE, 0.0025	7	0.13	1.67	440	0.25
0.18Cu,Na-MOR/7	LIE, 0.005	7	0.18	2.39	450	0.29
0.28Cu,Na-MOR/7	LIE, 0.01	7	0.28	3.73	450	0.25
0.34Cu,Na-MOR/7	LIE, 0.02	7	0.34	4.46	450	0.25

[1] determined by EDX on pressed pellets at 20 kV, error n_{Si}/n_{Al} ratio better ±5%, n_{Cu}/n_{Al} ±7%.

[2] determined at $p/p_0 = 0.99$

^{27}Al MAS NMR spectroscopy was applied for investigating the dealumination of the parent zeolite frameworks (see Figure S5 in the SI). NH_4-, H- and Na-MOR parent zeolites show a peak at 55 ppm

which is assigned to tetrahedrally coordinated framework aluminum (FAl). However in their H-forms after calcination at 823 K both parent H-MOR zeolites show a second peak around 0 ppm in their ^{27}Al MAS NMR spectra which is not the case for Na-MOR zeolites even after severe heat treatment (see Figure S6 in the SI). This peak is assigned to octahedrally coordinated extra-framework aluminum (EFAl). For the zeolites H-MOR/11 and H-MOR/7 evaluation of EFAl lead to quantities of ~12% and ~19% of the total aluminum content, respectively (see Figure S5 in the SI). Conclusively, the H-MOR parent zeolites contain significant amounts of EFAl species, in line with estimations from FT-IR by Grundner et al.[7]. To reveal the effect of the treatment at low pH (stirring over night between pH 5.2 and 5.7) without copper salt on the framework of parent H-MOR zeolites, ^{27}Al MAS NMR spectroscopy was applied (see Figure S7 in the SI). After the pH-treatment, the EFAl peak around 0 ppm is notably reduced in both n_{Si}/n_{Al} ratios while the n_{Si}/n_{Al} ratios determined from elemental composition (EDX) remain constant. This indicates a realumination of the mordenite framework in line with observations of Oumi et al.[36] Conversely to H-forms, if a heat treatment (30 h at 823 K, see Figure S6 in the SI) is applied to the Na-form of the zeolite, it shows a comparable ^{27}Al MAS NMR spectra as before the pH treatment.

Summarizing, no dealumination is observed on the sodium-exchanged zeolites while a significant de- and realumination is evidenced upon heat and/or pH treatment for H-MOR zeolites. The Na^+ counter ion stabilizes Si(ONa)Al groups relative to the Si(OH)Al groups which easily release and reinsert aluminum. This conclusion for H-MOR zeolites is supported by the work of Müller et al.[37], and similar effects are known from other zeolites.[12, 38]

3.2. The state of copper and Cu-MOR zeolite properties after ion exchange

A library of Cu-MOR materials was characterized by means of X-ray diffraction (XRD), N_2 physisorption, scanning electron microscopy (SEM) and energy dispersive X-ray spectroscopy (EDX). An overview over synthesis conditions and physicochemical properties can be found in Table 1. All materials were ion exchanged at a controlled pH (5.2 – 5.7) using solutions of copper acetate (0.0025 to 0.02 M) and afterwards properly washed. Multiple exchanges led to brownish MOR materials and thus to nanoparticle formation. This was also previously reported by Le et al.[15] after use of Cu,H-MOR materials prepared with high copper loadings by SSIE (above 1 wt% copper). Grundner et al.[7] used comparable exchange conditions as in this report, however, the investigated mordenite parent was supplied by Clariant. The n_{Si}/n_{Al} ratio of our mordenites did not change upon liquid ion exchange (LIE) or solid state ion exchange (SSIE) in their protonic or sodium forms. Thus no aluminum has been dissolved during the copper introduction. The LIE of Na-MOR zeolites with copper is more efficient than the exchange of H-MOR zeolites. Note that copper

exchanged Na-form zeolites contain minor amounts of Brønsted acid sites.[39-40] However, a higher copper concentration in the H-MOR materials through LIE was achieved with exchange solution of higher concentration. As it was evidenced by EDX, the materials contained no chlorine after SSIE with $CuCl_2$ (see Figure 1 below) and after SSIE with $CuAc_2$ and calcination no remaining carbon was evident. All materials are blueish and the color intensity increases with the density of copper ions. XRD patterns of all materials show a maintained mordenite framework without competing structures or significant amorphous contributions (see Figure S1 in the SI). No reflections of bulk copper at 2θ values of 35.5° and 38.7° are observed and thus bulk copper is absent.

N_2-physisorption revealed a correlation between equivalent BET surface area and counter ion content. The parent H-MOR had a significantly higher value for the equivalent BET surface area than the Na-MOR, independent of n_{Si}/n_{Al} ratios and by introducing copper a decrease in the equivalent BET surface area of the materials in accordance with previous observations was observed.[7, 41] The decrease (up to 12% of initial BET surface area) is not linearly correlated with the counter ion amount and can also be caused by dealumination of the H-MOR materials (see section 3.1 and Figure S5 in the SI). A small decrease in equivalent BET surface area was observed with the parent Na-MOR/11 or in general when SSIE was applied (compared to LIE). This hints to a better accessibility of the SSIE materials. Similar observations to the equivalent BET surface area can be made for the total volume V_{tot} which is in line with observations of Le et al.[15] Summarizing, counter ions present in MOR materials reduce the accessible inner surface area of the materials. Therefore, the exchange between Na^+ and Cu^{2+} is less affecting the inner surface than the exchange of Cu^{2+} for protons. For H-MOR materials, a SSIE procedure is in general resulting in slightly higher inner surfaces in form of equivalent BET surface area and total pore volume than a LIE.

The Cu-MOR materials prepared by LIE were investigated by SEM and BSE (see Figure S3 in the SI). Because of the small particle size, also here the use of EDX for the determination of the material composition is justified. In the BSE images of Cu-MOR materials 0.24Cu,H-MOR/7 and 0.36Cu,H-MOR/11 no bright spots of copper nanoparticles were evident. An in depth investigation using scanning electron microscopy (SEM), high angle backscattered electron detection (BSE), and energy-disperse X-ray spectroscopy (EDX) on the SSIE material 0.35Cu,H-MOR/11/Cl is illustrated in Figure 1. The investigated agglomerate has a diameter of approximately 20 μm and an uneven surface (see Figure 1a and 1b). A comparable investigation was conducted on samples after subsequent methane-to-methanol reaction cycles and can be found in Figure S4 in the SI.

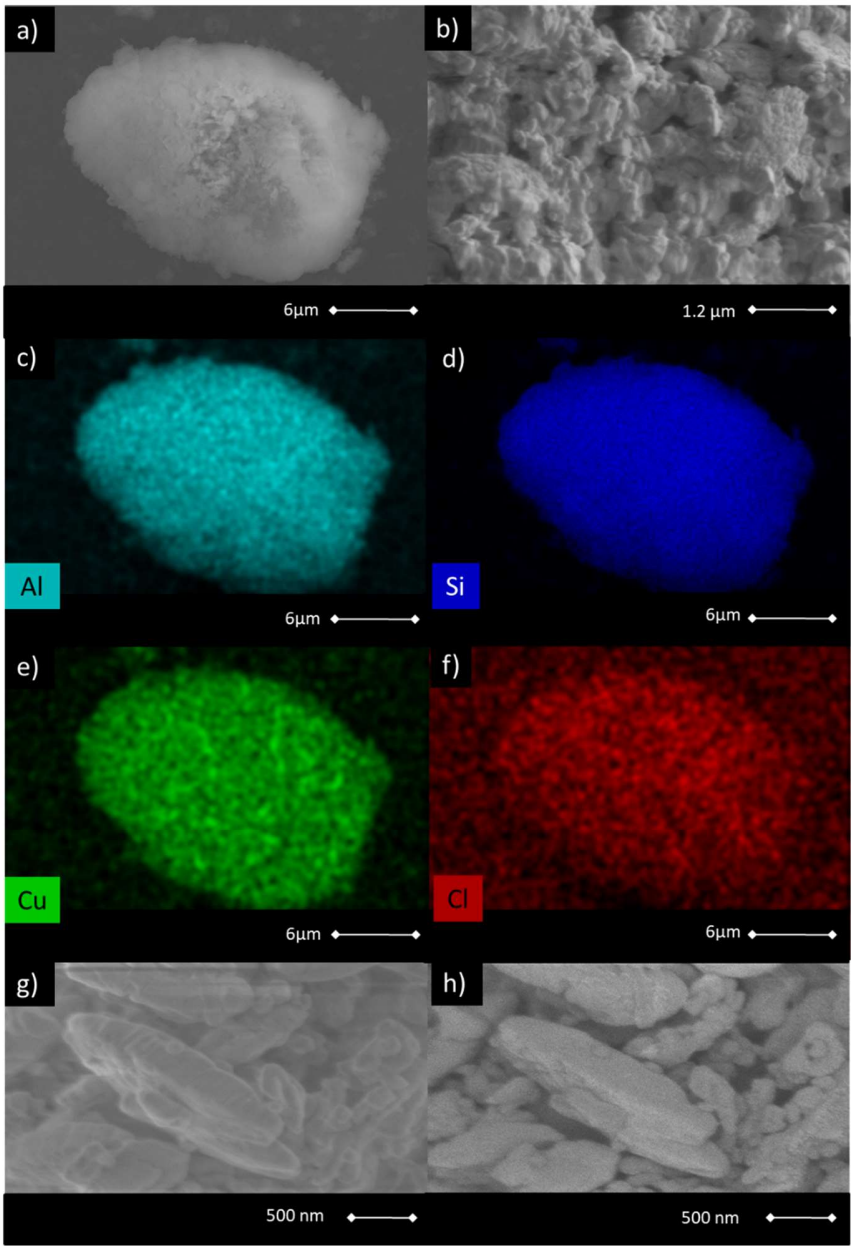

Figure 1: SEM and EDX investigations on 0.35Cu,H-MOR/11/Cl. SEM image of a crystal agglomerate (a) and detail of the agglomerate surface (b). EDX mapping shows an equal distribution of aluminum (c), silicon (d) and copper (e) throughout the agglomerate. Brighter spots are due to the rough surface of the agglomerate, as seen in (b). The mapping of chlorine (f) indicates a similar distribution of spots on agglomerate and background and thus the absence of chlorine on the material. Investigating the material with high resolution SEM (g) and BSE (h) shows that no agglomeration of copper is present.

Utilizing EDX we mapped the surface of particles to investigate the distribution of elements before reaction. The detected intensities are affected by the geometry of the surface as seen in Figure 1b. In Figures 1c to 1f, a mapping of aluminum, silicon, copper and chlorine are shown. The zeolite structure itself contains aluminum and silicon, so it is not surprising that these elements are omnipresent and equally distributed. It is furthermore obvious from Figure 1e that all copper is within the accuracy of this method equally distributed over the particles. According to previous findings of Grundner et al.[7], and within our detection limits, no changes in copper distribution and no nanoparticles appear after the methane activation reaction (not shown). In Figure 1f, the signal of chlorine was mapped and the signal vanishes in the background, confirming the absence of residual chlorine in the materials. High resolution SEM and BSE images of the 0.35Cu,H-MOR/11/Cl material are shown in Figure 1g and 1h, respectively. Formed CuO nanoparticles would result in an enhanced backscattering and bright spots on the material surface, as demonstrated elsewhere.[12] This confirms the absence of CuO nanoparticles in the material after SSIE with $CuCl_2$ down until ~10 nm, limited by the resolution of the BSE images taken and the same is true for the LIE materials (found in Figure S3 in the SI). Investigation of the materials after the methane-to-methanol conversion gave no indication of nanoparticle formation (see Figure S4 in the SI). Presence of stable copper sites and absence of nanoparticles is furthermore supported by the stable methane-to-methanol conversion performance (see section 3.3).

Summarizing, we were able to synthesize four different series of Cu-MOR materials, with variation of n_{Si}/n_{Al} ratio (7 or 11) and counter ion (H or Na). These materials do not contain copper nanoparticles, neither after synthesis nor after reaction, which was confirmed by XRD, EDX and BSE images as well as their optically visible color. All materials show a decrease in equivalent BET surface area and total pore volume in the dimension of up to 15% after a LIE with copper. In contrast to the LIE derived MOR materials, the equivalent BET surface area is maintained after SSIE with copper.

3.3. Performance in the methane-to-methanol reaction

The synthesized Cu- MOR materials were evaluated with respect to their methanol productivity as depicted in Figure 2. Tabulated values can be found in Table S1 in the SI. The conversion of methane to methanol was conducted in a stepwise manner. The performance of the materials synthesized via LIE with different counter ion, n_{Si}/n_{Al} ratio and n_{Cu}/n_{Al} ratio are depicted in Figure 2. Figure 2a shows the CH_3OH yield (µmol/g) as a function of Cu loading (µmol/g) and Figure 2b the normalized methanol productivity represented in mol_{CH3OH}/mol_{Cu} as a function of n_{Cu}/n_{Al} ratio.

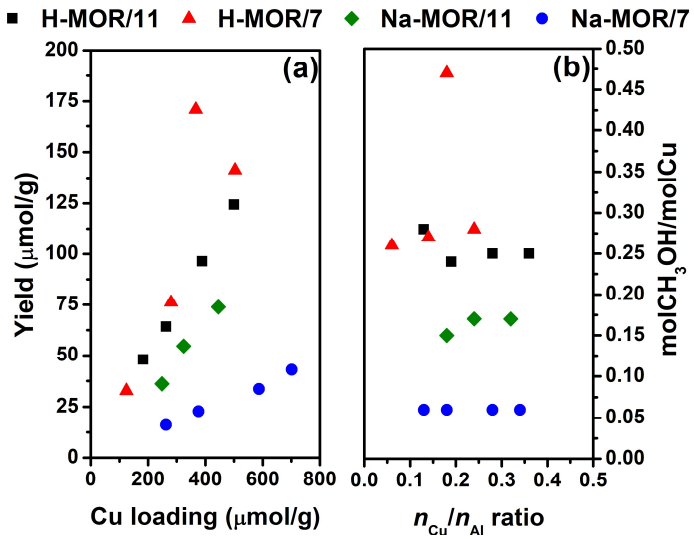

Figure 2: Performance of Cu-MOR materials prepared by LIE in the stepwise conversion, plotted per weight in µmol/g (left) and per copper in mol_{CH3OH}/mol_{Cu} (right). The calculated error in methanol yield is ± 3 %. Up to three independent measurements were conducted per point.

Evidently, all Cu-MOR materials possess the ability to convert methane to methanol. A linear trend between methanol productivity and copper content is observed. This indicates a uniform distribution of active Cu sites within the materials. The slopes indicate a significantly higher activity of the *x*Cu,H-MOR compared to the *x*Cu,Na-MOR materials. The corresponding slopes of *x*Cu,Na-MOR materials with n_{Si}/n_{Al} ratio 7 and 11 are 0.16 and 0.07, respectively. The selectivity towards methanol (see Table S1 in the SI) varies in between 84 and 92%, whereby materials with low n_{Cu}/n_{Al} ratio show lower selectivity. This can be interpreted as a threshold of unselective Cu sites that needs to be overcome. The methanol productivity in terms of mol_{CH3OH}/mol_{Cu} of Na-MOR materials of different n_{Si}/n_{Al} ratio extends the findings of Grundner et al.[14] The authors exchanged MOR materials with various counter ions (mono- and divalent) and found that the materials exhibit comparable activity as seen for our samples in Figure 2 at constant n_{Si}/n_{Al} ratio. However, changing the n_{Si}/n_{Al} ratio of Na^+ exchanged material alters the performance. On the other hand for the H-MOR derived materials we monitored a comparable activity in both n_{Si}/n_{Al} ratios, in accordance with findings of Grundner et al.[7] Our findings support that the proton counter ion is beneficial for the activity of the materials. Conversely, if few protons are present like on Na-MOR materials the activity is relatively low. The lower productivity of Na-MOR derived materials was previously explained by a competition in between Na^+ and Cu^{2+} counter ions.[14] We give another possible explanation for this differences in section 3.4. An outstanding methanol productivity of 169 µmol/g is found for a

*x*Cu,H-MOR/7 material with $x = 0.18$ in Figure 2, which equals a normalized productivity of 0.47 mol_{CH3OH}/mol_{Cu}. This is comparable to the 160 µmol/g reported by Grundner et al.[7], whereby the normalized productivity was 0.31-0.33 mol_{CH3OH}/mol_{Cu}. For 0.18Cu,H-MOR/7 this excludes a single site copper center of more than two copper atoms. Interestingly, the enhanced activity is observed at an intermediate point of copper exchange, meaning that not even half of the possible exchange sites are occupied by copper. For this report, we synthesized the respective material twice from scratch and found a reproducible activity (the value of 169.1 µmol/g is an average of both materials). We conclude, that an optimization of n_{Si}/n_{Al} ratio and n_{Cu}/n_{Al} ratio is possible. We suggest that the high productivity of the 0.18Cu,H-MOR/7 material is the result of combining a certain aluminum distribution distribution (influenced by both zeolite synthesis conditions and n_{Si}/n_{Al} ratio) with a fitting copper loading. A peaking productivity furthermore points to multiple reaction regimes, e.g. in low loadings copper active site inhibition, in high copper loadings overoxidation or to the presence of multiple active sites. In a recent study, with have applied high-energy resolution XANES and multivariate curve resolution analysis to resolve the contributions from such active and inactive Cu(II) moieties, thereby proving the presence of di-copper active sites in a selection of the LIE H-MOR materials studied. [4]

*x*Cu,H-MOR materials with comparative n_{Cu}/n_{Al} ratio ($x \approx 0.1$ and 0.35) derived from both LIE and from SSIE (with $CuCl_2$ respectively $CuAc_2$ as copper source) were evaluated with respect to their methanol productivity over multiple reaction cycles in Figure 3. Again, the left side shows yield as µmol/g material and right the normalized productivity mol_{CH3OH}/mol_{Cu}.

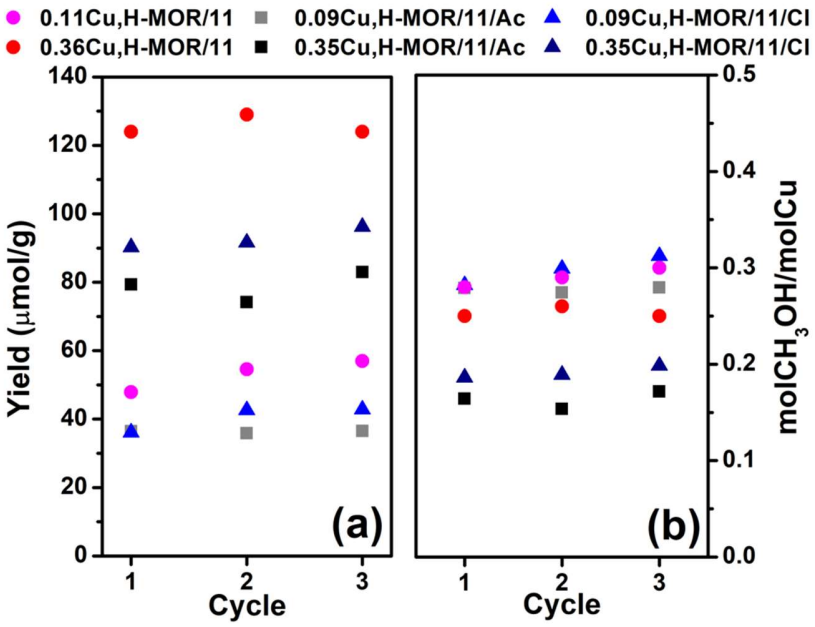

Figure 3: Methanol yield of LIE and SSIE MOR materials with low and high copper loading, respectively, over 3 subsequent reaction cycles. The methanol yield error is ± 3 %, with up to three measurements conducted per point.

In the case of $CuCl_2$ the SSIE reaction is driven by HCl formation during the inert gas treatment. On the other hand for $CuAc_2$ the organic anion required an oxygen calcination step. This was followed by an inert gas treatment, performed in order to exclude that the copper distribution is influenced by self-reduction (monovalent charged Cu^{I} ions are because of their lower charge weaker bond to the surface and more mobile than twofold charged Cu^{II} ions). However, it turns out that the materials prepared by LIE outperform the SSIE derived ones. Among the materials prepared by SSIE, the samples derived from the organic copper salt ($CuAc_2$) exhibit a smaller normalized methanol productivity. This is most evident in a high Cu loading ($x \approx 0.35$) and in the first process cycle. High and low Cu loading materials exhibit a decreasing methanol productivity (see Table S1 in the SI) in the order LIE > SSIE ($CuCl_2$) > SSIE ($CuAc_2$).

For all the tested materials a quasi-stable performance is exhibited. Just a slight increase in methanol productivity (less than 10%) is observed when moving to the next cycle. Note that Le et al.[15] used $Cu^{I}Cl$ for the exchanges leading to less productive Cu-MOR materials and therefore supported the use of $Cu^{II}(acac)_2$. Furthermore, for mordenites derived from SSIE a strong increase in activity after multiple reaction cycles was previously reported.[16] Taking that into account, it is evident that our

materials show an initially high copper distribution coming close to the final distribution state. A comparable distribution could in other studies[16] be achieved after performing multiple reaction cycles. The strong improvements reported there are thus a result of the over stoichiometric exchange with $Cu^{I}Cl$, leading to an inhomogeneous copper distribution and nanoparticles formed on H-MOR parents that contain possibly large amounts of EFAl. It is conclusive that EFAl located in the pores blocks them partially and hinders the copper ions distribution during the SSIE.

Summarizing, the methanol productivity depends on the parent materials as well as on the copper exchange routes. H-MOR derived materials show a better productivity compared to Na-MOR based ones. For the H-MOR based materials, the n_{Si}/n_{Al} ratio seems of minor importance whereas for the Na-form derived ones the methanol productivity is influenced by this parameter. Among the exchange routes, LIE outperforms SSIE routes after one, two, and three reaction cycles. Among the SSIE routes, the exchange with $CuCl_2$ outperformed the exchange with $CuAc_2$. Taking into account our results and the literature, we strongly advise not to use $Cu^{I}Cl$ in a SSIE of MOR zeolites for the methane-to-methanol conversion and support instead the LIE route using H-MOR parents and a Cu^{II} salt at a pH <6. The methanol productivity of all herein investigated materials is rather stable throughout the investigated reaction cycles and the performed characterization (see also next section) hinting to a stable Al-Cu distance, corresponding to a constant copper distribution. At a n_{Cu}/n_{Al} ratio of x = 0.18 for the xCu,H-MOR/7, a 0.47 mol_{CH3OH}/mol_{Cu} productivity was observed indicating an optimum balance between Cu loading and Cu location leading to a high population of active sites.

3.4 Structural stability investigated by ^{27}Al and ^{29}Si MAS NMR spectroscopy

^{27}Al MAS NMR (see Figure 4) and ^{29}Si MAS NMR (see Table 2) spectroscopy was applied to investigate the zeolite framework stability during the conversion cycles.[24, 42] We evaluated the degree of dealumination and the framework n_{Si}/n_{Al}-ratio by ^{29}Si MAS NMR using Löwenstein's rule.[22-27, 34] Data from the ^{27}Al MAS NMR spectra can be found in Table S2 in the SI, while the ^{29}Si MAS NMR spectra can be found in Figure S8 in the SI. We start with a discussion of ^{27}Al MAS NMR spectra. A signal intensity loss is frequently observed due to paramagnetic wipe-out of nuclei close to copper.[34] Herein, we saw an intensity loss of up to 16% in the highest copper exchange degree for the materials 0.24Cu,H-MOR/7.

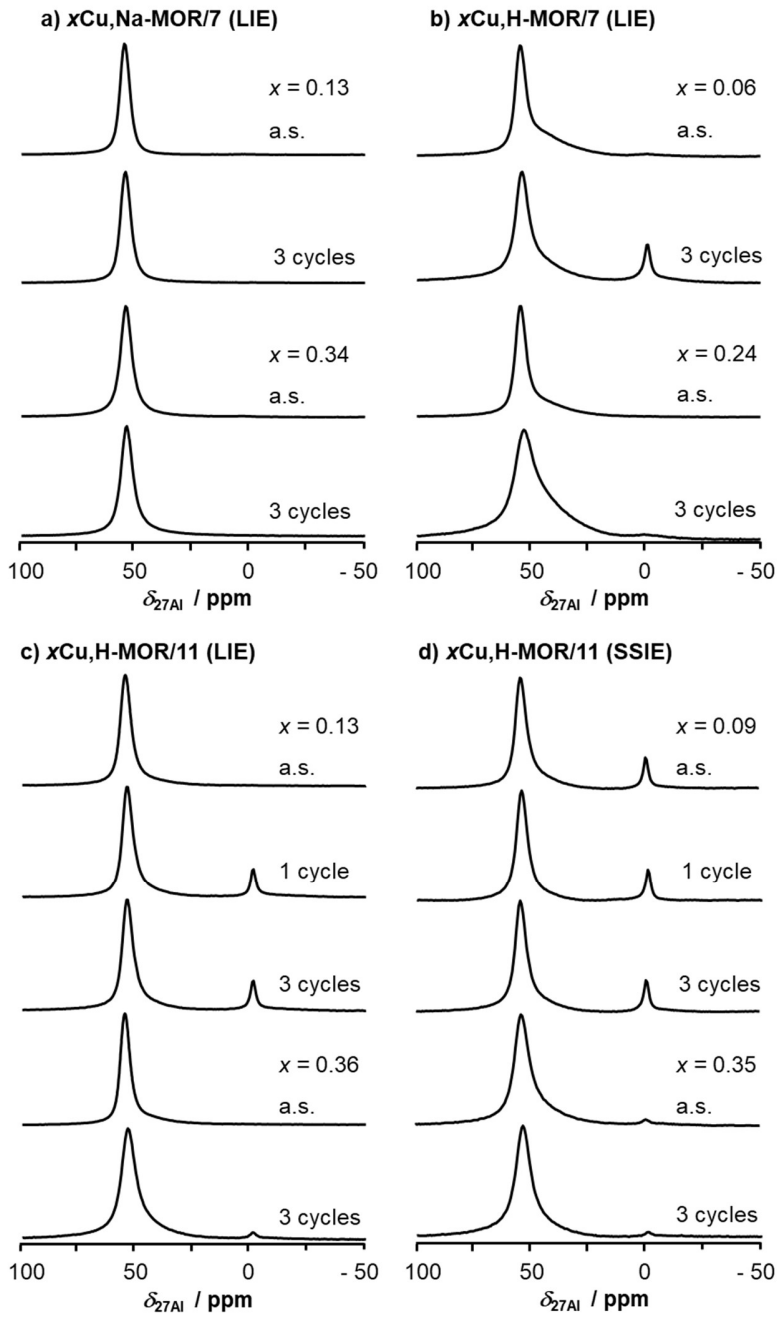

Figure 4: ^{27}Al MAS NMR spectra of the copper containing MOR materials before and after up to 3 reaction cycles. Peaks at 55 ppm are assigned to tetrahedral framework aluminum, peaks at 0 ppm to extra framework aluminum (EFAl). Mordenites ion exchanged by a SSIE approach using $CuCl_2$ and $CuAc_2$ show identical spectra as the LIE derived H-MOR materials. For peak area ratios and FWHM refer to Table S2 in the SI. For enlarged spectra including spinning sidebands please refer to Figure S12 in the SI.

The ^{27}Al MAS NMR spectra of *x*Cu,Na-MOR/7 materials with low (x = 0.13) and high (x = 0.34) copper loadings are shown in Figure 4a. Peaks appear exclusively at 55 ppm, assigned to tetrahedral framework aluminum while no EFAl characterized by a peak around 0 ppm is visible. The aluminum incorporation is maintained after three consecutive reaction cycles. Note that a comparable degree of dealumination is achieved after one or more reaction cycles and after a harsh heat treatment in air, indicating the dealumination has reached a final state (see Figure S9 in the SI). A graph on reaction cycles on *x*Cu,Na-MOR/11 materials can be found in Figure S10 in the SI.

In Figure 4b ^{27}Al MAS NMR spectra of *x*Cu,H-MOR/7 materials with low (x = 0.06) and high (x = 0.24) copper loadings are shown. A peak around 0 ppm (EFAl species) is observed on the hydrated high copper loaded material (x=0.24) after 3 reaction cycles, and a weak peak at 0 ppm is observed in the as-synthesized material for x = 0.06 (2% of total ^{27}Al signal intensity, see Table S2 in the SI). The peaks at 55 ppm seen in figure 4b all have a broad feature to their right. This feature is likely due to framework distortions generated during sample preparation steps and subsequent reaction cycles. The significant broadening of the x = 0.24 material's peak at 55 ppm is comparable to the broadening observed in Cu-Y materials.[31] Distorted tetrahedral Al species are likely the origin to these features.

As-synthesized LIE materials with n_{Si}/n_{Al}-ratio 11 found in Figure 4c show no EFAl. However, EFAl is formed after the first reaction cycle and accounts for a constant 10% of aluminum during 3 reaction cycles (see Table S2 in the SI). For higher copper loadings (x = 0.36) the peak at 0 ppm is less intense and accounts for just 2% of the ^{27}Al total signal intensity after 3 reaction cycles. This can be rationalized by framework stabilization due to Cu^{2+} counter ions similar to the stabilization by Na^{+} counter ions discussed above. The peak at 55 ppm does not significantly broaden upon applying multiple cycles (see Table S2 in the SI), consistent with a stable zeolite framework.

Two materials with n_{Si}/n_{Al}-ratio 11 prepared by SSIE with $CuCl_2$ (*x*Cu,H-MOR/11/Cl) were investigated by ^{27}Al MAS NMR spectroscopy with low (x = 0.09) and high (x = 0.35) copper loadings are shown in Figure 4d. Interestingly, the as-synthesized material with low Cu (x=0.09) show a peak around 0 ppm indicating that the EFAl species in the parent zeolites (see SI Figure S5) are in part maintained after the SSIE. This is conclusive since no pH treatment was conducted (see Figure S7 in the SI for the influence of pH treatment). EFAl blocking the pores of parent H-MOR zeolites might prevent a homogeneous distribution of the copper ions, explaining the inferior methanol productivity. Furthermore the content of EFAl in the x = 0.35 material is remarkably low about 2%, but constant throughout 3 cycles (see Table S2 in the SI). The same is true for the 12% EFAl on the 0.09Cu,H-MOR/11/Cl (see Figure S7 and Table S2 in the SI). The peak at 55 ppm of

this low copper loaded mordenite stays similar for up to 3 reaction cycles. Generally, it seems that EFAl species are present when there is a high methane-to-methanol output of Cu-MOR. However, their presence before ion exchange may prevent a homogeneous distribution of copper in the MOR framework. The EFAl itself might have a stabilizing effect on active species or moderate the oxidation of methane. However, the exact reason for the better performance of EFAl containing materials remains, based on the present data, speculative.

A fundamental difference in between ^{27}Al and ^{29}Si MAS NMR spectroscopy is the distance of the nuclei under observation to the copper: In case of ^{27}Al all atoms are located close to the pore and the Cu^{2+}, whereas 3 of 4 Q4(1Al) ^{29}Si atoms are located twice as far away from the Cu^{2+}. Noteworthy, the total ^{29}Si MAS NMR signal intensity of our spectra (weight corrected, error ± 5%) is maintained upon copper exchange. In other words in our ^{29}Si spectra we see no intensity loss due to paramagnetic copper and thus no signal wipe-out is observable. We estimated the spin-lattice T1 time constant in the highest copper loaded sample (0.24Cu,H-MOR/11) to be below 0.2 s (see Figure S11 in the SI). It is in accordance with literature that paramagnetic copper shortens the T1 relaxation time.[31-33, 43] All evaluated ^{29}Si MAS NMR spectra, sum of simulated peaks and single peaks are shown in Figure S8 in the SI. The EFAl content and the associated theoretical FW n_{Si}/n_{Al} ratio of parent zeolites and of Cu-MOR materials after 3 reaction cycles derived from ^{27}Al and ^{29}Si MAS NMR spectroscopy are summarized in Table 2.

Table 2: Dealumination of MOR materials after burning off ammonia (parent zeolites) and after 3 reaction cycles evaluated by ^{27}Al and ^{29}Si MAS NMR spectroscopy. The data is derived from Figure S5 and Table S2 in the SI (^{27}Al) and from Figure S8 in the SI (^{29}Si). The expected framework (FW) n_{Si}/n_{Al} ratio is calculated from the EDX total n_{Si}/n_{Al} ratio (error better ±5%) taking into account the EFAl content from ^{27}Al MAS NMR (error ±5%, minimum 1; for details on calculation see [12]). The error of the ^{29}Si spectra analysis according to Lippmaa et al. [24] is ± 5%).

material	% EFAl content (^{27}Al)	FW n_{Si}/n_{Al} ratio (^{27}Al and EDX) [26]	FW n_{Si}/n_{Al} ratio (^{29}Si)
H-MOR/7	19	8.6 ± 0.5	8.8 ± 0.4
0.06Cu,H-MOR/7	12	8.0 ± 0.5	8.4 ± 0.4
0.24Cu,H-MOR/7	2	7.1 ± 0.4	6.8 ± 0.3
0.13Cu,Na-MOR/7	0	7.0 ± 0.4	6.6 ± 0.3
H-MOR/11	12	12.5 ± 0.8	11.5 ± 0.6
0.11Cu,H-MOR/11	10	12.2 ± 0.7	11.2 ± 0.6
0.36Cu,H-MOR/11	2	11.2 ± 0.7	10.4 ± 0.5

0.09Cu,H-MOR/11/Cl	12	12.5 ± 0.8	10.9 ± 0.6
0.35Cu,H-MOR/11/Cl	2	11.2 ± 0.7	10.8 ± 0.5

The FW n_{Si}/n_{Al}-ratio derived from ^{29}Si MAS NMR spectroscopy was calculated from the amount of Q4 silicon with 0Al, 1Al, and 2Al neighbors according to the shift ranges known from literature.[22, 24] Note here, that for weakly dealuminated high silica mordenites (n_{Si}/n_{Al}-ratio 11) a second Q4(0Al) T-site was partially visible, as expected for a framework with multiple T-sites and demonstrated by Fyfe et al.[22] for high-silica zeolites. Nevertheless, trends can be observed that fully support the ^{27}Al MAS NMR investigations. Parent H-MOR zeolites have the highest FW n_{Si}/n_{Al} ratio and the highest EFAl content, whereas high copper loading materials have a low FW n_{Si}/n_{Al} ratio and less EFAl species. In particular for the 0.13Cu,Na-MOR/7 no significant dealumination occurs and the FW n_{Si}/n_{Al} ratio is the smallest observed. Comparable results were gained for materials with the n_{Si}/n_{Al}-ratio 11. This proves that the FW n_{Si}/n_{Al}-ratio decreases with increasing copper content and supports findings from ^{27}Al MAS NMR spectroscopy.

Until now a dealumination was assumed to be absent[21] or the dealumination quantity was averaged.[7] However, we show that Cu-MOR materials have a rather complex de- and realumination chemistry that has to be accounted for in the models, including material-depending dealumination degrees. It is furthermore interesting to note that possible electronic paramagnetic centers located on Cu are very likely not influencing the peak positions and shapes, as it was also reported previously for example by Inagaki et al.[32] The (Cu-)electron dipole-(^{27}Al or ^{29}Si-) nuclei dipole interaction is weak, as we see no line broadening or any spinning sideband manifold different than expected from non-Cu samples.. Also, if paramagnetic copper would influence the quantification, one would expect a strong discrepancy in between evaluation of ^{27}Al or ^{29}Si signals because of the larger distance of ¾ of Q4 ^{29}Si nuclei to the copper. This is clearly not the case. The direct Fermi contact interaction must also be of minor importance since we do not observe any peak shifts from the usual positions for ^{27}Al and ^{29}Si. However, the spin-lattice relaxation time/recovery time of Si (see below) is heavily shortened as a results of Cu ions in the materials.

From our findings using ^{27}Al and ^{29}Si MAS NMR spectroscopy we see that a dealumination of *x*Cu,H-MOR materials occurs when used in the methane-to-methanol conversion. The quantity of the dealumination and EFAl formation is associated with the counter ions, and thus the copper loading of H-form mordenites. As-synthesized *x*Cu,H-MOR materials prepared by LIE show a weak peak at 0 ppm attributed to some EFAl present in the framework as result of the pH-treatment during

copper exchange and the introduction of stabilizing copper counter ions. With Na-MOR parent and without previous dealumination, *x*Cu,Na-MOR materials show no EFAl present neither after synthesis nor after reaction. Significant amounts form however, in *x*Cu,H-MOR materials after just one reaction cycle. The observed EFAl content is constant over 3 reaction cycles. At higher copper loadings, the copper protects the mordenite framework from any significant dealumination. For the synthesis of Cu-MOR by SSIE, the presence of EFAl in as-synthesized mordenites has to be taken into account. These species hinder the homogeneous copper distribution and results thereby in less productive zeolites. All highly productive materials contain significant amounts of EFAl species in their pores.

4. Conclusion

Copper mordenites (Cu-MOR) show a broad performance variety in the methane-to-methanol conversion that depends on the material properties. Key factors for the methanol productivity are nature of copper accompanying counter ions and the copper ion exchange procedure. Liquid ion exchange (LIE) of the H-MOR parents at a pH between 5.2 and 5.7 generates the most productive Cu-MOR materials. No benefits of solid state ion exchanges (SSIE) are found. The *x*Cu,H-MOR activity is independent of n_{Si}/n_{Al} ratio and stays below 0.3 mol_{CH3OH}/mol_{Cu} with one exception for a zeolite with n_{Si}/n_{Al} ratio 7 and n_{Cu}/n_{Al} ratio 0.18. This material shows a reproducible methanol productivity of up to 0.47 mol_{CH3OH}/mol_{Cu} with a selectivity of up to 92% as a result of an optimum stoichiometry between framework silicon, aluminum, and copper counter ions. No copper oxide nanoparticle formation was observed on the materials and the methanol productivity was stable over three reaction cycles. This is explained by an initially high copper distribution inside the MOR zeolite pores. The LIE treatment at a pH in the range 5.2 to 5.7 leads to a realumination of the mordenite framework. All *x*Cu,H-MOR materials show dealumination during the reaction cycles, since the water extraction step equals to a steaming procedure. The quantity of extra-framework aluminum (EFAl) species formed on *x*Cu,H-MOR decreases with increasing counter ion quantity. It is thereby not relevant for the framework stabilization if the present counter ion is Na or Cu. The quantity of formed EFAl is maintained during subsequent reaction cycles. We show that the quantity of the dealumination can be investigated by ^{27}Al MAS NMR and ^{29}Si MAS NMR spectroscopy with comparable accuracy. ^{27}Al Signals of EFAl were observable and exhibited neither broadening nor shifting. No intensity loss but strong paramagnetic signal enhancement was observed in case of ^{29}Si MAS NMR spectroscopy. It is important to note that the more active Cu-MOR materials show strong EFAl formation. This EFAl benefits the methanol productivity for a reason that remains speculative. However, the EFAl must be taken into account when reactivity data are analyzed stoichiometrically, e.g. methanol is related to n_{Cu}/n_{Al} ratios.

Acknowledgements

This publication forms a part of the iCSI (industrial Catalysis Science and Innovation) Center for Research-based Innovation, which receives financial support from the Research Council of Norway under contract no. 237922.

We thank K. A. Lomachenko, G. Berlier, S. Bordiga, K. P. Lillerud, and C. Lamberti for insightful discussions and for their support to the research project.

Supporting Information.

Contains XRD patterns, SEM and BSE images, EDX mappings, additional ^{27}Al and ^{29}Si MAS NMR measurements as well as tabulated data.

References

1. Groothaert, M. H.; Smeets, P. J.; Sels, B. F.; Jacobs, P. A.; Schoonheydt, R. A., Selective Oxidation of Methane by the Bis(í-oxo)dicopper Core Stabilized on ZSM-5 and Mordenite Zeolites. *J. Am. Chem. Soc.* **2005,** *127*, 1394-1395.
2. Alayon, E. M.; Nachtegaal, M.; Bodi, A.; Ranocchiari, M.; van Bokhoven, J. A., Bis(mu-oxo) versus mono(mu-oxo)dicopper cores in a zeolite for converting methane to methanol: an in situ XAS and DFT investigation. *PCCP* **2015,** *17*, 7681-7693.
3. Alayon, E. M. C.; Nachtegaal, M.; Bodi, A.; van Bokhoven, J. A., Reaction Conditions of Methane-to-Methanol Conversion Affect the Structure of Active Copper Sites. *ACS Catal.* **2014,** *4*, 16-22.
4. Pappas, D. K.; Martini, A.; Dyballa, M.; Kvande, K.; Teketel, S.; Lomachenko, K. A.; Baran, R.; Glatzel, P.; Arstad, B.; Berlier, G.; Lamberti, C.; Bordiga, S.; Olsbye, U.; Svelle, S.; Beato, P.; Borfecchia, E., The nuclearity of the active site for methane to methanol conversion in Cu-mordenite: a quantitative assessment. *J. Am. Chem. Soc.* **2018**, DOI: 10.1021/jacs.8b08071 (in press).
5. Vanelderen, P.; Snyder, B. E.; Tsai, M. L.; Hadt, R. G.; Vancauwenbergh, J.; Coussens, O.; Schoonheydt, R. A.; Sels, B. F.; Solomon, E. I., Spectroscopic definition of the copper active sites in mordenite: selective methane oxidation. *J Am Chem Soc* **2015,** *137*, 6383-92.
6. Vanelderen, P.; Vancauwenbergh, J.; Tsai, M. L.; Hadt, R. G.; Solomon, E. I.; Schoonheydt, R. A.; Sels, B. F., Spectroscopy and redox chemistry of copper in mordenite. *ChemPhysChem* **2014,** *15*, 91-9.
7. Grundner, S.; Markovits, M. A.; Li, G.; Tromp, M.; Pidko, E. A.; Hensen, E. J.; Jentys, A.; Sanchez-Sanchez, M.; Lercher, J. A., Single-site trinuclear copper oxygen clusters in mordenite for selective conversion of methane to methanol. *Nat. Commun.* **2015,** *6*, 7546.
8. Palagin, D.; Knorpp, A. J.; Pinar, A. B.; Ranocchiari, M.; van Bokhoven, J. A., Assessing the relative stability of copper oxide clusters as active sites of a CuMOR zeolite for methane to methanol conversion: size matters? *Nanoscale* **2017,** *9*, 1144-1153.
9. Park, M. B.; Ahn, S. H.; Mansouri, A.; Ranocchiari, M.; van Bokhoven, J. A., Comparative Study of Diverse Copper Zeolites for the Conversion of Methane into Methanol. *ChemCatChem* **2017,** *9*, 3705-3713.

10. Ipek, B.; Wulfers, M. J.; Kim, H.; Göltl, F.; Hermans, I.; Smith, J. P.; Booksh, K. S.; Brown, C. M.; Lobo, R. F., Formation of [Cu2O2]2+ and [Cu2O]2+ toward C–H Bond Activation in Cu-SSZ-13 and Cu-SSZ-39. *ACS Catal.* **2017,** *7*, 4291-4303.
11. Pappas, D. K.; Borfecchia, E.; Dyballa, M.; Pankin, I. A.; Lomachenko, K. A.; Martini, A.; Signorile, M.; Teketel, S.; Arstad, B.; Berlier, G.; Lamberti, C.; Bordiga, S.; Olsbye, U.; Lillerud, K. P.; Svelle, S.; Beato, P., Methane to Methanol: Structure-Activity Relationships for Cu-CHA. *J. Am. Chem. Soc.* **2017,** *139*, 14961-14975.
12. Dyballa, M.; Pappas, D. K.; Borfecchia, E.; Beato, P.; Olsbye, U.; Lillerud, K. P.; Arstad, B.; Svelle, S., Tuning the material and catalytic properties of SUZ-4 zeolites for the conversion of methanol or methane. *Micro. Meso. Mater.* **2018,** *265*, 112-122.
13. Borfecchia, E.; Pappas, D. K.; Dyballa, M.; Lomachenko, K. A.; Negri, C.; Signorile, M.; Berlier, G., Evolution of active sites during selective oxidation of methane to methanol over Cu-CHA and Cu-MOR zeolites as monitored by operando XAS. *Catalysis Today* **2018**, DOI: 10.1016/j.cattod.2018.07.028 (in press).
14. Grundner, S.; Luo, W.; Sanchez-Sanchez, M.; Lercher, J. A., Synthesis of single-site copper catalysts for methane partial oxidation. *Chem. Commun.* **2016,** *52*, 2553-2556.
15. Le, H. V.; Parishan, S.; Sagaltchik, A.; Göbel, C.; Schlesiger, C.; Malzer, W.; Trunschke, A.; Schomäcker, R.; Thomas, A., Solid-State Ion-Exchanged Cu/Mordenite Catalysts for the Direct Conversion of Methane to Methanol. *ACS Catal.* **2017,** *7*, 1403-1412.
16. Bozbag, S. E.; Alayon, E. M. C.; Pecháček, J.; Nachtegaal, M.; Ranocchiari, M.; van Bokhoven, J. A., Methane to methanol over copper mordenite: yield improvement through multiple cycles and different synthesis techniques. *Cat. Sci. & Tech.* **2016,** *6*, 5011-5022.
17. Tomkins, P.; Mansouri, A.; Bozbag, S. E.; Krumeich, F.; Park, M. B.; Alayon, E. M.; Ranocchiari, M.; van Bokhoven, J. A., Isothermal Cyclic Conversion of Methane into Methanol over Copper-Exchanged Zeolite at Low Temperature. *Angew. Chem. Int. Ed.* **2016,** *55*, 5467-5471.
18. Haag, W. O.; Lago, R. M.; Weisz, P. B., The active site of acidic aluminosilicate catalysts. *Nature* **1984,** *309*, 589.
19. Jiang, Y.; Huang, J.; Dai, W.; Hunger, M., Solid-state nuclear magnetic resonance investigations of the nature, property, and activity of acid sites on solid catalysts. *Solid State Nucl Magn Reson* **2011,** *39*, 116-41.
20. Blasco, T.; Boronat, M.; Concepcion, P.; Corma, A.; Law, D.; Vidal-Moya, J. A., Carbonylation of methanol on metal-acid zeolites: evidence for a mechanism involving a multisite active center. *Angew. Chem. Int. Ed.* **2007,** *46*, 3938-3941.
21. Narsimhan, K.; Michaelis, V. K.; Mathies, G.; Gunther, W. R.; Griffin, R. G.; Roman-Leshkov, Y., Methane to acetic acid over Cu-exchanged zeolites: mechanistic insights from a site-specific carbonylation reaction. *J. Am. Chem. Soc.* **2015,** *137*, 1825-1832.
22. Fyfe, C. A.; Gobbi, G. C.; Klinowski, J.; Thomas, J. M.; Ramdas, S., Resolving crystallographically distinct tetrahedral sites in silicalite and ZSM-5 by solid-state NMR. *Nature* **1982,** *296*, 530.
23. Klinowski, J.; Thomas, J. M.; Fyfe, C. A.; Hartman, J. S., Applications of magic-angle-spinning silicon-29 nuclear magnetic resonance. Evidence for two different kinds of silicon-aluminum ordering in zeolitic structures. *The Journal of Physical Chemistry* **1981,** *85*, 2590-2594.
24. Lippmaa, E.; Mägi, M.; Samson, A.; Tarmak, M.; Engelhard, G., Investigation of the Structure of Zeolites by Solid-state High-Resolution 29Si NMR Spectroscopy. *J. Am. Chem. Soc.* **1981,** *103*, 4992-4996.
25. Ripmeester, J. A.; Majid, A.; Hawkins, R. E., Magic angle spinning29Si and27Al NMR study of mordenite dealumination. *Journal of inclusion phenomena* **1983,** *1*, 193-198.
26. Engelhard, G., Solid State NMR Spectroscopy Applied to Zeolites. In *Studies in Surface Science and Catalysis*, van Bekkum, H.; Flanigen, E. M.; Jansen, J. C., Eds. Elsevier: Amsterdam, 1991; Vol. 58, pp 285-315.
27. Fyfe, C. A.; Thomas, J. M.; Klinowski, J.; Gobbi, G. C., Magic-Angle-Spinning NMR (MAS-NMR) Spectroscopy and the Structure of Zeolites. *Angewandte Chemie International Edition in English* **1983,** *22*, 259-275.

28. Li, W.; Celinski, V. R.; Weber, J.; Kunkel, N.; Kohlmann, H.; Schmedt auf der Günne, J., Homogeneity of doping with paramagnetic ions by NMR. *Physical Chemistry Chemical Physics* **2016,** *18*, 9752-9757.
29. Grey, C. P.; Dupré, N., NMR Studies of Cathode Materials for Lithium-Ion Rechargeable Batteries. *Chemical Reviews* **2004,** *104*, 4493-4512.
30. Beale, A. M.; Gao, F.; Lezcano-Gonzalez, I.; Peden, C. H. F.; Szanyi, J., Recent advances in automotive catalysis for NOx emission control by small-pore microporous materials. *Chemical Society Reviews* **2015,** *44*, 7371-7405.
31. Zhou, L.; Li, S.; Su, Y.; Li, B.; Deng, F., Paramagnetic relaxation enhancement solid-state NMR studies of heterogeneous catalytic reaction over HY zeolite using natural abundance reactant. *SS Nucl. Magn. Reson.* **2015,** *66-67*, 29-32.
32. Inagaki, S.; Kawamura, I.; Sasaki, Y.; Yoshida, K.; Kubota, Y.; Naito, A., Drastic sensitivity enhancement in 29Si MAS NMR of zeolites and mesoporous silica materials by paramagnetic doping of Cu2+. *Physical Chemistry Chemical Physics* **2013,** *15*, 13523-13531.
33. Palamara, J.; Seidel, K.; Moini, A.; Prasad, S., Ion distribution in copper exchanged zeolites by using Si-29 spin lattice relaxation analysis. *J. Magn. Reson.* **2016,** *267*, 9-14.
34. Song, J.; Wang, Y.; Walter, E. D.; Washton, N. M.; Mei, D.; Kovarik, L.; Engelhard, M. H.; Prodinger, S.; Wang, Y.; Peden, C. H. F.; Gao, F., Toward Rational Design of Cu/SSZ-13 Selective Catalytic Reduction Catalysts: Implications from Atomic-Level Understanding of Hydrothermal Stability. *ACS Catal.* **2017,** *7*, 8214-8227.
35. Kresnawahjuesa, O.; Gorte, R. J.; de Oliveira, D.; Lau, L. Y., A Simple, Inexpensive, and Reliable Method for Measuring Brønsted-Acid Site Densities in Solid Acids. *Catalysis Letters* **2002,** *82*, 155-160.
36. Oumi, Y.; Nemoto, S.; Nawata, S.; Fukushima, T.; Teranishi, T.; Sano, T., Effect of the framework structure on the dealumination–realumination behavior of zeolite. *Materials Chemistry and Physics* **2003,** *78*, 551-557.
37. Müller, M.; Harvey, G.; Prins, R., Comparison of the dealumination of zeolites beta, mordenite, ZSM-5 and ferrierite by thermal treatment, leaching with oxalic acid and treatment with SiCl4 by 1H, 29Si and 27Al MAS NMR. *Micro, Meso, Mater,* **2000,** *34*, 135-147.
38. Dyballa, M.; Obenaus, U.; Lang, S.; Gehring, B.; Traa, Y.; Koller, H.; Hunger, M., Brønsted sites and structural stabilization effect of acidic low-silica zeolite A prepared by partial ammonium exchange. *Micro. Meso. Mater.* **2015,** *212*, 110-116.
39. Li, Y.; Hall, W. K., Catalytic decomposition of nitric oxide over Cu-zeolites. *J. Catal.* **1991,** *129*, 202-215.
40. Parrillo, D. J.; Dolenec, D.; Gorte, R. J.; McCabe, R. W., Adsorption Studies on Cu-ZSM-5: Characterization of the Unique Properties of Ion-Exchanged Cu. *J. Catal.* **1993,** *142*, 708-718.
41. Narsimhan, K.; Iyoki, K.; Dinh, K.; Roman-Leshkov, Y., Catalytic Oxidation of Methane into Methanol over Copper-Exchanged Zeolites with Oxygen at Low Temperature. *ACS Cent. Sci.* **2016,** *2*, 424-429.
42. Kanellopoulos, J.; Unger, A.; Schwieger, W.; Freude, D., Catalytic and multinuclear MAS NMR studies of a thermally treated zeolite ZSM-5. *J. Catal.* **2006,** *237*, 416-425.
43. Zhou, L.; Li, S.; Qi, G.; Su, Y.; Li, J.; Zheng, A.; Yi, X.; Wang, Q.; Deng, F., Methanol carbonylation over copper-modified mordenite zeolite: A solid-state NMR study. *SS Nucl. Magn. Reson.* **2016,** *80*, 1-6.